Chapter 5

AFM studies on Langmuir-Blodgett films of cholesterol

5.1 Introduction

An understanding of the assembly and deposition of cholesterol (Ch) is important in biology. Ch is found in eukaryotic cell membranes, as byproducts during the bio-synthesis of bile acid and in blood plasma. It plays an important role in many biological activities [1, 2]. Cholesterol molecules are transported in the blood plasma through proteins known as lipoproteins. In the process of its transportation, the free Ch gets deposited on the arterial wall. Such nucleation and deposition leads to the formation of atherosclerotic lesions in the arterial and coronary walls [3]. Recently, Abendan and Swift [4] have studied the surface properties of single crystal cholesterol monohydrate in solutions using atomic force microscope (AFM) and chemical force microscope. They have reported a plate like structure and the thinnest plate to be a bilayer. The Ch molecules when spread at the air-water (A-W) interface, assemble to yield a stable Langmuir monolayer. The monolayer of Ch at the A-W interface exhibits a condensed phase with the long molecular axis oriented normal to the interface [5, 6]. Lafont *et al*. [5] have studied the Ch monolayer deposited on mica using AFM. They have found that the film of Ch on mica at lower surface pressure (3 mN/m) was an uniform homogeneous layer of monomolecular thickness. On the other hand, at higher surface pressure (20 mN/m), they have observed elongated thick domains.

In this chapter, we describe our AFM studies on the assembly of Ch molecules deposited

by LB technique on different substrates. The substrates were treated chemically to yield well defined hydrophobic or hydrophilic surfaces prior to the film deposition. The monolayer of Ch in the condensed phase was transferred on the solid substrates. The aggregation and the assembly of Ch in the films were studied using atomic force microscope (AFM) in the tapping mode.

5.2 Experimental

The experimental details for studying the Ch monolayer at the A-W interface using surface manometry, Brewster angle, and epifluorescence microscopy were similar as discussed in the previous chapters.

The hydrophilic substrates were prepared using optical quality glass plates which were boiled in piranha solution [7] (3:1, conc H_2SO_4:H_2O_2) for 5 minutes and then rinsed successively with ultrapure ion-free water, absolute alcohol and acetone solvents. The substrates were then dried by blowing hot air at 70 °C. To prepare the hydrophobic substrates, the piranha treated substrates were immersed in a 10% solution of 1,1,1,3,3,3-hexamethyldisilazane (HMDS) in HPLC grade chloroform for about 12 hours. The substrates were taken out and rinsed successively with chloroform and ion-free water. The hydrophobicity of the substrates thus prepared were reasonably good with a contact angle greater than 90°. Metal coated glass plates were also used as hydrophilic substrates. They were obtained by the deposition of thermally evaporated metals on glass plates at a pressure of about 10^{-6} Torr. The substrates were annealed for 30 minutes at a temperature of 300 °C prior to the metal evaporation. We prepared the LB films of Ch on gold, aluminium and platinum coated substrates. In the case of gold, a thin layer (around 200 Å) of chromium was used as an adhesion promoter. The thickness of the gold film was estimated to be around 2500 Å.

The target surface pressure (π_t) for the LB deposition was chosen at 30 mN/m which was within the monolayer regime (Figure 5.1). On attaining the target surface pressure (30 mN/m), the monolayer was allowed to equilibrate for 15 minutes. Each cycle of

deposition consisted of one downstroke and one upstroke of the dipper. The dipper speed was maintained at 10 mm/min and 5 mm/min for the downward and upward motion, respectively. The speed during the upward motion was made relatively slower to facilitate drainage of water trapped between the layers. Corrections for the thickness of the substrates and the meniscus were taken into account while calculating the transfer ratio. The AFM studies were undertaken using NanoScope IIIa (Digital Instruments). For the imaging, silicon (Si) tips were used. The spring constants were in the range of 0.1-0.6 N/m. Si gets oxidized in air and forms a thin film of SiO_2. This contributes to the hydrophilicity of the tip [8]. Tapping mode has numerous advantages over contact mode for imaging soft matter and biological samples [9]. All the AFM images presented here were taken in the tapping mode. The Scanning Probe Image Processor (SPIP) software was used to analyze the images.

5.3 Results and Discussion

The surface pressure (π) - area per molecule (A_m) isotherm for Ch is shown in Figure 5.1. Ch monolayer at the A-W interface is known to exhibit gas phase, untilted condensed (L_2) phase and collapsed state [5, 10].

The BAM and epifluorescence images show a very uniform gray texture in the L_2 phase of the Ch monolayer, and these are shown in Figure 5.2.

We have transferred the Ch monolayer on substrates by LB technique at various surface pressures. We find the transfer efficiency was much better at 30 mN/m compared to those at lower surface pressures like 3, 10 and 20 mN/m. Also, at surface pressures greater than 30 mN/m, the monolayer approaches the collapse state and hence not very stable for the deposition. Thus we have chosen a target surface pressure (π_t) of 30 mN/m. This is nearly in the middle of the steep region of the isotherm and is well within the L_2 phase. Figure 5.2 shows the epifluorescence and BAM images taken at a surface pressure of 30 mN/m. Both the images show an uniform L_2 phase. We have attempted to transfer the monolayer films on both hydrophobic and hydrophilic substrates. We find that the first layer gets deposited efficiently on both kind of substrates. However, we were not able to transfer more than

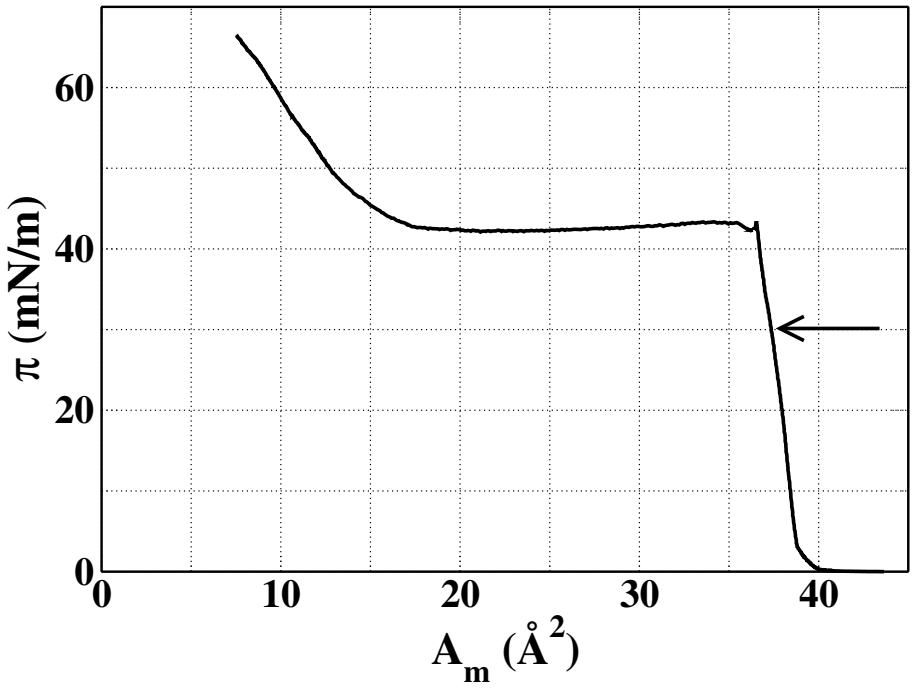

Figure 5.1: Surface pressure (π) - area per molecule (A_m) isotherm of Ch monolayer. The steep region of the isotherm, in the range of about 36.5-38.5 Å^2, corresponds to the untilted condensed (L_2) phase. The LB film was transferred at the target surface pressure of 30 mN/m, as indicated by the arrow.

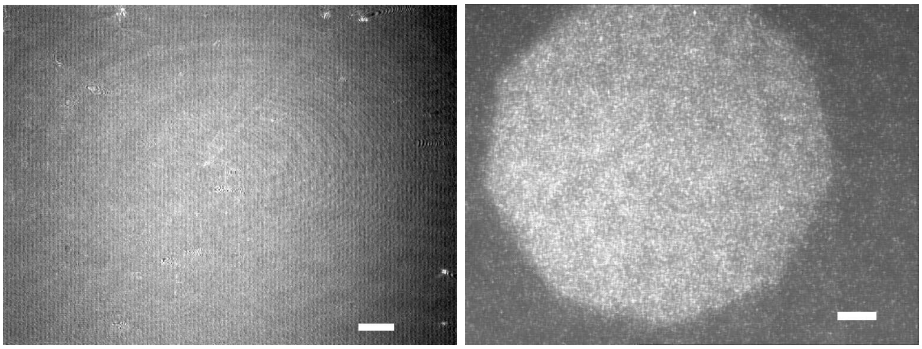

(a) (b)

Figure 5.2: (a) and (b) show the BAM and epifluorescence images, respectively, of the cholesterol (Ch) monolayer captured at a surface pressure of 30 mN/m (π_t). (a) and (b) show a very uniform gray texture representing the L_2 phase. The scale bars in (a) and (b) correspond to 500 μm and 50 μm, respectively.

one layer on hydrophilic substrates. This was due to the fact that for every upstroke and downstroke of the dipper, the molecules get adsorbed and desorbed by equal amounts. Ch molecule is largely hydrophobic in nature. Hence, the interaction between the hydrophilic substrates and the Ch molecules are weak to support the multilayer formation during the LB deposition. On the other hand, the Ch molecules exhibited much better adhesion on HMDS treated hydrophobic glass substrates. During LB transfer on the HMDS treated hydrophobic substrates, we observed the X-type of deposition, where adsorption takes place only during the downstroke *i.e.*, when the substrate was immersing into the subphase. The transfer efficiency of the LB film is denoted by the transfer ratio (τ) which is the ratio of the area of the monolayer removed from the A-W interface during deposition to the area of the substrate to be deposited (please see chapter 1 for detail description of τ). We find that the very first monolayer gets deposited efficiently where the τ was always 1±0.02. Contrarily, for upstrokes there was some desorption. During each cycle of deposition, it was clear from the transfer ratio data (Figure 5.3) that downstrokes adsorb the molecules efficiently while the upstrokes desorb fraction of the earlier deposited layers. This shows that though the

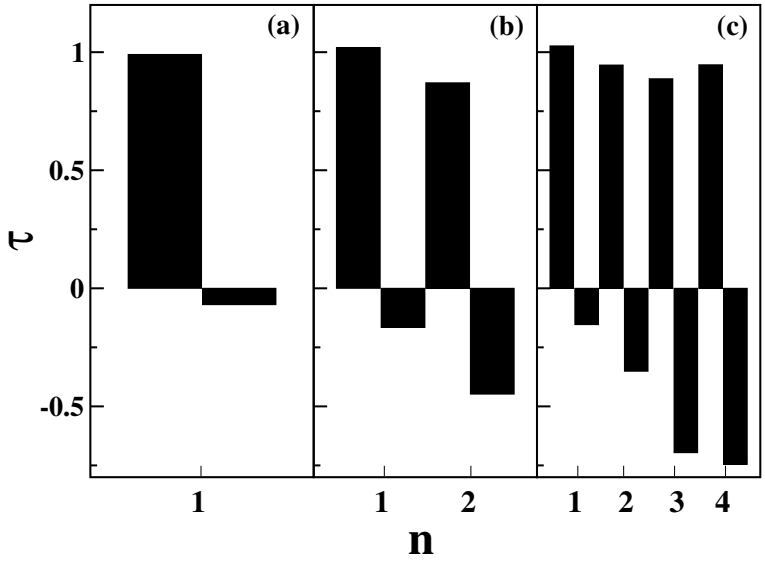

Figure 5.3: The transfer ratio (τ) data as a function of number of cycles (n) of LB deposition of Ch on hydrophobic substrates. (a), (b) and (c) represent one, two and four cycles of LB deposition. In each cycle, the two bars represent the transfer ratio (τ) of one downstroke and one upstroke of deposition. The positive and negative transfer ratio data indicate the adsorption and desorption of the molecules, respectively. One can see that during the downstrokes, there are adsorption while during upstrokes there are some desorption. The desorption increases with increasing number of cycles of deposition.

interaction between the hydrophobic substrate and the Ch molecule was strong, the layer to layer interaction was weaker to support multilayer formation. We define the effective adsorption on the substrate as $\eta_n = S_n/\rho_t$ where S_n is the net surface concentration on the substrate after n^{th} cycle and ρ_t is the surface concentration (inverse of A_m) of the monolayer at A-W interface at π_t. The variation of the effective adsorption with the number of cycles of deposition is shown in Figure 5.4. It is evident from the transfer ratio data (Figure 5.3)

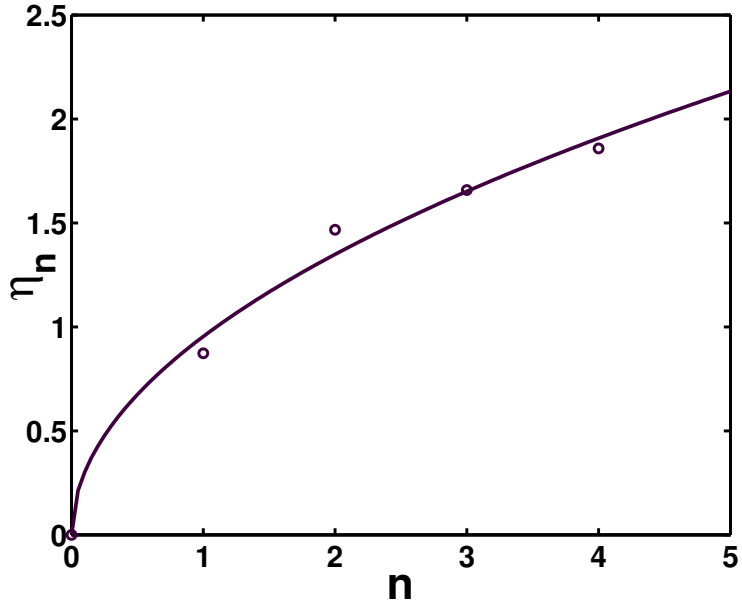

Figure 5.4: The effective adsorption η_n is plotted with respect to number of cycles of deposition (n). The experimental data is represented by the open circles (**o**). The continuous line is a guide for the eye.

that the desorption becomes significant after the first cycle of deposition. Also, beyond four cycles of deposition, the desorption was almost equal to that of adsorption, resulting in the saturation of effective adsorption, η_n. Hence, it can be inferred that the interaction between the Ch-Ch layers is weaker as compared to that of the hydrophobic substrate-first layer of Ch. The adsorption of one layer of Ch on another layer during LB transfer can lead to defects due to weak layer to layer interaction. These defects can act as nucleation sites for further desorption of the molecules during upstrokes. With increasing cycles of deposition, the filling of the defects and reorganization of the molecules may yield patterns observed in AFM imaging.

The AFM images of the HMDS treated hydrophobic substrate for the two different scan ranges are shown in Figure 5.5. Both the images show a very uniform texture at two different length scales. The height profile data of the AFM image for a scan range of 200×200 nm^2

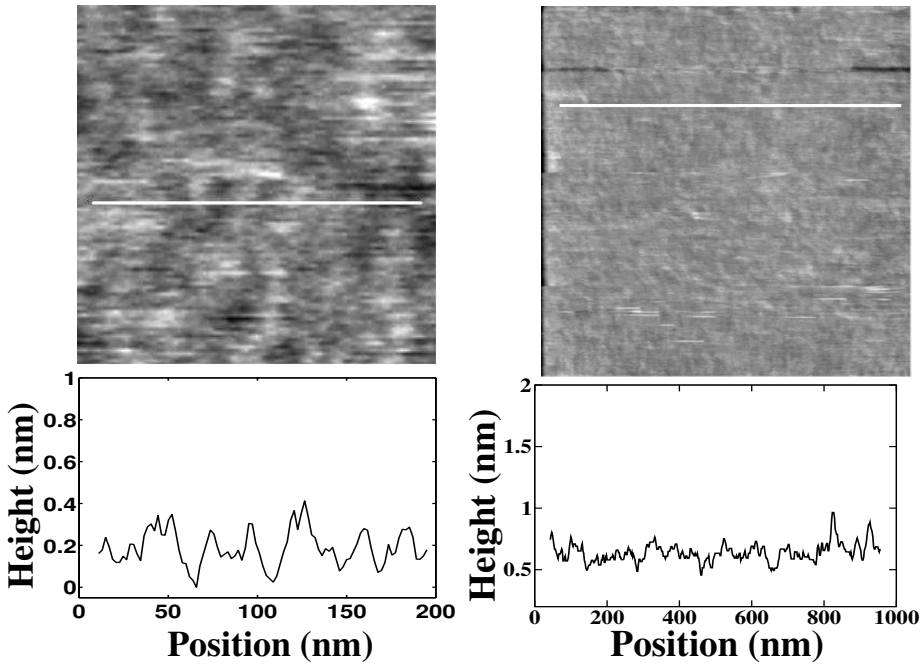

(a) 200×200 nm^2 (b) 1×1 μm^2

Figure 5.5: AFM images of HMDS treated hydrophobic reference glass substrate at two different scan ranges. The white lines on the images are drawn to measure the height variation along it. The corresponding height profiles are shown below the respective images.

(Figure 5.5(a)) showed the average height variation to be 0.19 nm. The root mean square (RMS) roughness of the substrate was found to be 0.13 nm. This indicated the smoothness of the HMDS treated substrate compared to the untreated glass substrate which had a RMS roughness of about 1.9 nm. To show the uniformity of the substrate, an image of a larger scan range of 1×1 μm^2 is presented in Figure 5.5(b). The RMS roughness for this image was 0.65 nm. The difference in roughness between untreated glass substrate and HMDS treated glass substrate can be attributed to the homogeneous covering of the HMDS on the glass substrate rendering it very smooth.

The AFM images of the LB films of Ch on HMDS treated hydrophobic substrates with the respective height profiles along a chosen line are shown in Figures 5.6 and 5.7.

Figures 5.6(a) and 5.6(b) show the images for one cycle of the deposited film for scan ranges of 200×200 nm^2 and 1×1 μm^2, respectively. It is seen from the image (Figure 5.6(a)) that the

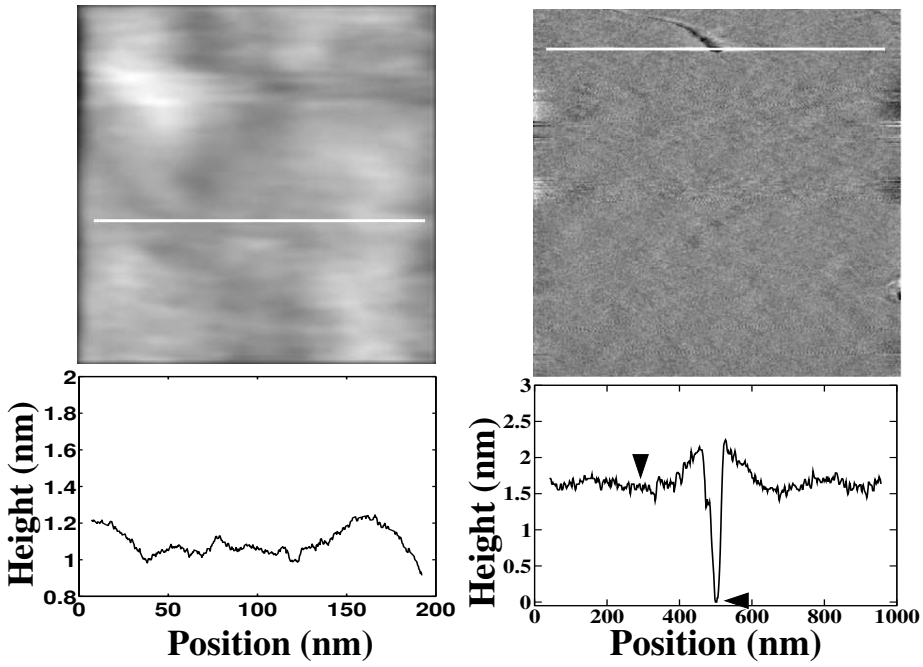

(a) 200×200 nm^2 (b) 1×1 μm^2

Figure 5.6: AFM images of the LB film of Ch on the hydrophobic substrate deposited during one cycle. The white line on the images is drawn to measure the height variation along it. The corresponding height profiles are shown below the respective images. In the height profile of (b), the arrows indicate the points which yield a height of 1.63 nm.

molecules form a homogeneous film with minor defects. Figure 5.6(b) shows a very uniform and homogeneous film with some defects at the top of the image. Such defects can be used to estimate the thickness of the films. Here drawing a line along a defect and measuring the height profile reveal a film of thickness of about 1.6 nm. This thickness corresponds to the length of a Ch molecule [11] along its long axis, indicating the film to be a layer of Ch molecules oriented normal to the substrate. This is consistent with the earlier AFM studies on mica [5]. We have also drawn height profiles at various positions along defects in other AFM images. Further, we have measured the differences between the maxima and minima in the height profiles and using such data along with the measurement over defects, we have estimated the thickness of the films. However, if the film is very uniformly covered

(Figure 5.6(a)), drawing a height profile is not sufficient to determine the thickness of the film. The height variation as a function of position (height profile) reveals the topography of the film and is useful in modeling the molecular arrangements. The height distribution in the AFM images are presented in Figure 5.8. Here each image was scanned from one end to another and the height value in each pixel was saved. By counting the number of pixels having a height value ranging within a defined bin, one can get the distribution of height in a particular image. The narrowing of the peak (Figure 5.8(a)) for one cycle of film, indicates the monodispersity of the height distribution. Figure 5.7(a) represents the image

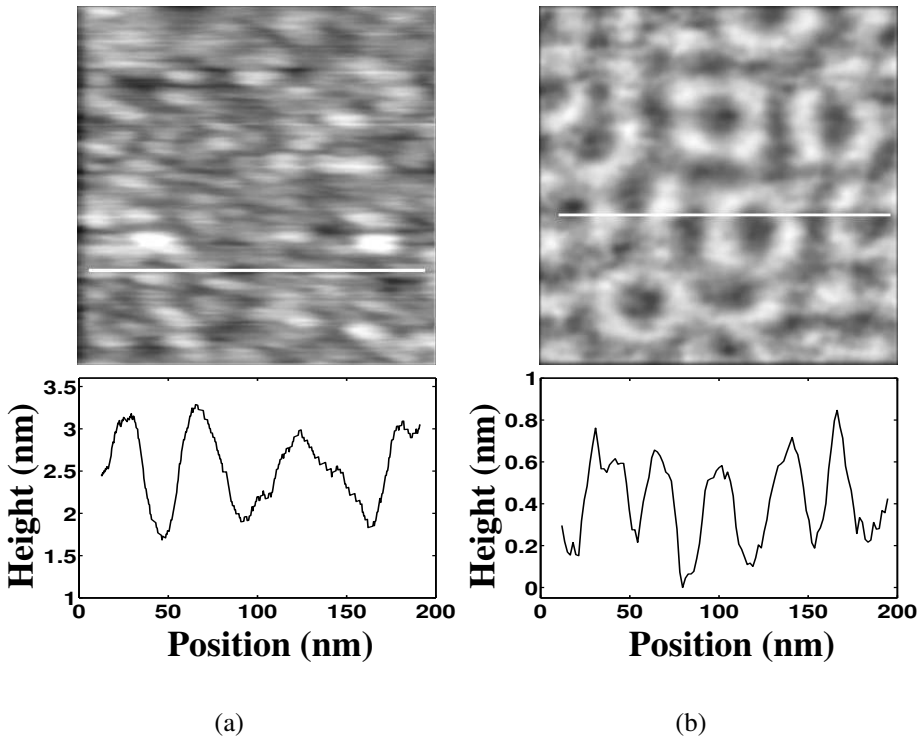

(a) (b)

Figure 5.7: (a) and (b) represent the LB films of cholesterol (Ch) molecules on the hydrophobic substrate deposited during two and four cycles, respectively. The white line on the images is drawn to measure the height variation along it. The corresponding height profiles are shown below the respective images. The image size in each case is 200×200 nm^2.

for the two cycles of deposited film. It shows the elongated domains. The histogram of the height distribution (Figure 5.8(b)) peaks at 3.0 nm which approximately corresponds to a bilayer. The height profile shown in Figure 5.7(a) reveals the average height variation to be about 1.6 nm. Thus it can be inferred that the elongated domains are the domains of single

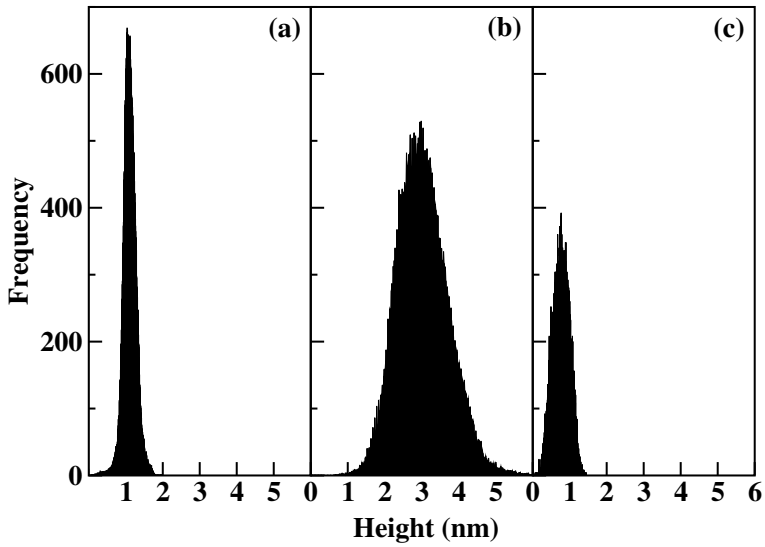

Figure 5.8: (a), (b) and (c) are the histograms of the height distribution of the AFM images shown in Figures 5.6(a), 5.7(a) and 5.7(b), respectively. Each AFM image is scaled to 256×256 pixels. The height value at each pixel was determined and used to plot the histogram. The bin size for (a), (b) and (c) are 0.004, 0.013 and 0.003 nm, respectively. The axes are chosen to be equal for comparison.

layer of normally oriented molecules on the top of another uniformly covered monolayer. Interesting features were seen in the image for four cycles of deposited film (Figure 5.7(b)). It shows an uniformly distributed torus shaped domains (doughnuts) having the average outer diameter of about 65 nm and annular width of about 22 nm. The average height variation of the torus, as measured from the height profile, is 0.56 nm. The corresponding histogram of the height distribution is shown in Figure 5.8(c). To avoid any instrumental artifacts we have checked the images by scanning at a larger length scale. We find consistency in the scaling of the torus shaped domains with the scaling of the scan range (Figures 5.9(a) and 5.9(c)). Figures 5.9(b) and 5.9(d) show the corresponding phase images which have been taken simultaneously with the height images during the tapping mode AFM. For the three cycles of deposition, the doughnut patterns were not very well developed and hence we have not analyzed them.

The calculated parameters of the AFM images are listed in Table 5.1.

The simultaneous height and phase imaging provide a qualitative insight about the mechanical and chemical nature of the system [12–14]. Raghavan *et al*. [8] have used the phase imaging tapping mode to study the blend of polystyrene (PS) and polybutadiene (PB)

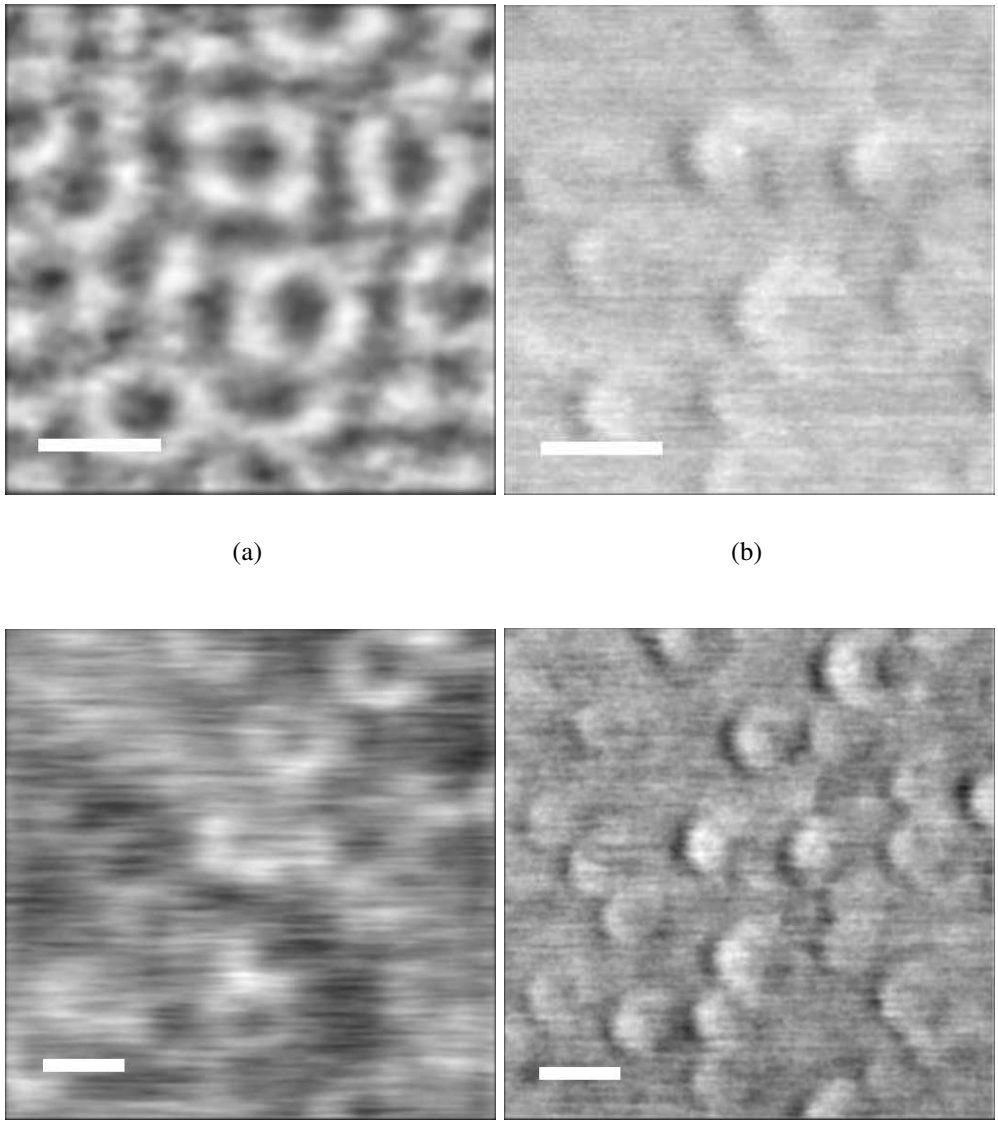

(a) (b)

(c) (d)

Figure 5.9: (a) and (c) represent the height images of the four cycles of deposition of Ch at two different scan ranges. Figures (b) and (d) are the corresponding phase images. The scale bar represents 50 nm.

Table 5.1: The calculated parameters of the AFM images. (For Figures 5.6(a) and 5.7 for the scan range of 200×200 nm^2)

	HMDS treated hydrophobic substrate (nm)	One cycle (nm)	Two cycles (nm)	Four cycles (nm)
Average roughness	0.1	0.13	0.54	0.18
RMS roughness	0.13	0.18	0.67	0.22
Histogram peaks at	-	1.1	3.0	0.8
FWHM of histogram	-	0.38	1.58	0.54
Average height variation	0.19	0.18	1.6	0.56

as a function of annealing time. They observed high contrast phase images which were primarily due to the differences in the mechanical and chemical properties of PS and PB. Annealing the system lead to an equilibration in the mechanical and chemical properties due to cross-linking and oxidation. They find that the height images revealed a high contrast between the domains, whereas the phase images revealed a poor contrast. This trend is clearly seen in their phase image for a 102 hours annealed polymer blend. The bright and dark regions in the phase images were attributed to the more polar and less polar regions, respectively, as probed by a hydrophilic tip [8]. We find a good contrast in the AFM height images, whereas a poor contrast in the phase images. The phase images show that the doughnuts are asymmetric and only one side gives dark and bright regions (Figures 5.9(b) and 5.9(d)). We find that this feature does not depend on scan direction. Similar phase images have been reported in literature [8]. The poor contrast in the phase images is likely due to a single component system, *i.e*. Ch film. To explain the dark regions in the phase images, we suggest that it corresponds to less polar regions of the LB film. The less polar regions may be due to flipping of the Ch molecules. Flipping of the molecules in the LB films of fatty acid using AFM has been reported [15, 16]. In the X-type of deposition, the molecules adsorb on the substrate with its hydrophilic group projecting away from the substrate. The bright background in the phase images indicates that the projection of polar -OH part of Ch is away from the substrate, whereas the darker region may be due to the branched non-polar hydrophobic methyl group of the flipped molecules.

The effective adsorption (η_n) for two layers of normally oriented molecules should be

two. However, for the two cycles and four cycles of deposited films, η_n is found to be 1.5 and 1.86, respectively (Figure 5.4). Taking this into account, we suggest that the average variation in height of 0.56 nm obtained from the height profile (Figure 5.7(b)) in the torus shaped domains is due to the gradual variation of tilt of the molecules with respect to the surface normal. Considering the length of the Ch molecule to be 1.6 nm, and the average height variation to be 0.56 nm, we get a value of about 50° for the maximum tilt of the Ch molecules. Figure 5.10 shows a schematic representation of the arrangement of molecules in the different cycles of LB deposition.

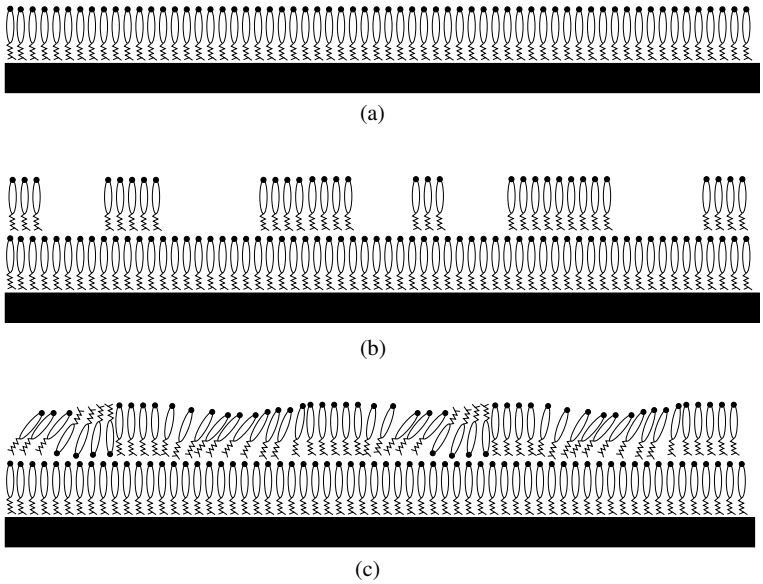

Figure 5.10: Schematic representation showing the cross-sectional view of a possible arrangement of the Ch molecules on the hydrophobic substrate. (a), (b) and (c) represent layer structure for one, two and four cycles of depositions, respectively. The filled circles represent the hydrophilic -OH of the molecule, the elliptical part represents the hydrophobic Ch skeleton and the rest is the iso-octyl chain of the molecule. The smooth homogeneous film of Ch obtained during one cycle of deposition (average height variation of 0.18 nm, obtained from Figure 5.6(a)) is shown by the normally oriented Ch molecules on the hydrophobic substrate (a). For the two cycles of deposition, the elongated domains of average height variation of 1.6 nm are shown by defects in the second layer over the homogeneously covered first layer (b). For the four cycles of deposition, the height variation of 0.56 nm in the torus shaped domains is accounted for by the tilt of the molecules by 50°. The dark region observed in the phase images of the torus shaped domains is accounted for by the flipping of the Ch molecules (c).

In the one cycle of deposition, we depict one layer of normally oriented Ch molecules (Figure 5.10(a)) consistent with the AFM image. In the two cycles of deposited film (Figure 5.10(b)), bunch of molecules separated by defects are drawn to illustrate the

elongated domains of thickness of a molecular length. The variation in height observed in the torus shaped domains (doughnuts) is accounted for by the gradual tilt of the molecules. The dark regions in the phase images in the doughnuts are accounted for by the flipping of the Ch molecules that yield a less polar region (Figure 5.10(c)).

The phenomenon of the effects of adsorption and desorption on the assembly and deposition of organic ultrathin films are of considerable interest. Nygren and Stenberg [17] have reported the kinetics of adsorption and desorption of ferritin molecules on hydrophobic substrate at liquid-solid interface. They find that the adsorption and desorption have a marked effect on the supramolecular assembly of the molecules. Though our system is different from theirs, one can find an analogy of adsorption and desorption giving rise to interesting patterns.

The aggregation of the molecules in the LB films are highly dependent on the nature of the substrates and the experimental parameters, such as dipper speed, temperature, pH, salts and relative humidity [18]. Sikes *et al*. [19] have reported that the relaxation of the molecules in the LB films of salts of fatty acid are due to the reorganization of the molecules in their thermodynamically stable states. The reorganization in the domains takes place due to the instability that sets in because of the drainage and evaporation of thin layer of entrapped water between the layers. Such an instability may cause the molecules to diffuse from one region to the other due to Marangoni flow [19]. The formation of the torus shaped domains in the LB films of Ch are due to the reorganization of the molecules on the hydrophobic substrate during adsorption and desorption.

5.4 Conclusions

We have found interesting patterns in the AFM images showing the assembly of Ch molecules during LB deposition. The first layer is a uniform homogeneous film of molecules in accordance with earlier reports [5]. The two cycles of deposition exhibits elongated domains on a uniformly covered film. The four cycles of deposition results in the aggregation of Ch molecules into torus shaped domains (doughnuts). Interestingly, these doughnuts

are very uniformly distributed. The transfer ratio for each cycle of deposition shows that adsorption is followed by some amount of desorption. The process of adsorption and desorption results in the assembly of Ch molecules into interesting structures. We find that the deposition of molecules were not possible beyond four cycles indicating a saturation in the effective adsorption.

Bibliography

[1] P. L. Yeagle, Biochim. Biophys. Acta **822**, 267 (1985).

[2] R. Lipowsky and E. Sackmann, *Structure and dynamics of the membranes* (North-Holland, Amsterdam, 1995).

[3] J.P. Segrest and G.M. Anantharamaiah, Curr. Opin. Cardiol. **9**, 404 (1994).

[4] R. S. Abendan and J. A. Swift, Langmuir **18**, 4847 (2002).

[5] S. Lafont, H. Rapaport, G.J. Sömjen, A. Renault, P.B. Howes, K. Kjaer, J. Als-Nielsen, L. Leiserowitz, and M. Lahav, J. Phys. Chem. B **102**, 761 (1998).

[6] P. Viswanath and K. A. Suresh, Phys. Rev. E **67**, 061604 (2003).

[7] Piranha solution is dangerous and to be handled carefully.

[8] D. Raghavan, X. Gu, T. Nguyen, M. VanLandingham, and A. Karim, Macromolecules **33**, 2573 (2000).

[9] P. K. Hansma, J. P. Cleveland, M. Radmacher, D. A. Walters, P. E. Hillner, M. Bezanilla, M. Fritz, D. Vie, H. G. Hansma, C. B. Prater, J. Massie, L. Fukunaga, J. Gurley, and V. Elings, Appl. Phys. Lett. **64**, 1738 (1994).

[10] J. P. Slotte, M. Jungner, C. Vilchèze, and R. Bittman, Biochim. Biophys Acta **1190**, 435 (1994).

[11] The length of cholesterol molecule along its long axis is 1.6 nm, as determined using ACD/ChemSketch, Freeware Version 5.12, Advanced Chemistry Development, Inc., Toronto ON, Canada, www.acdlabs.com, 2002.

[12] Ph. Leclère, R. Lazzaroni, J. L. Brédas, J. M. Yu, Ph. Dubois, and R. Jèrôme, Langmuir **12**, 4317 (1996).

[13] S. N. Magonov, V. Elings, and M. -H. Whangbo, Surf. Sci. **375**, L385 (1997).

[14] A.Noy, C. H. Sanders, D. V. Vezenov, S. S. Wong, and C. M. Leiber, Langmuir **14**, 1508 (1998).

[15] D. Y. Takamoto, E. Aydil, J. A. Zasadzinski, A. T. Ivanova, D. K. Schwartz, T. Yang, and P. S. Cremer, Science **293**, 1292 (2001).

[16] D. K. Schwartz, Surf. Sci. Rep. **27**, 241 (1997).

[17] H. Nygren and M. Stenberg, Biophys. Chem. **38**, 67 (1990); **38**, 77 (1990).

[18] J. A. Zasadzinski, R. Viswanathan, L. Madsen, J. Garnaes, and D. K. Schwartz, Science **263**, 1726 (1994).

[19] H. D. Sikes, J. T. Woodward, and D.K. Schwartz, J. Phys. Chem. **100**, 9093 (1996).